Res Chem Intermed (2018) 44:1275–1293
https://doi.org/10.1007/s11164-017-3166-2

Inhibition effects of orange peel extract on the corrosion of Q235 steel in CO_2-saturated and CO_2/H_2S coexistent brine solutions

Chen Zhang[1] · Jingmao Zhao[1,2]

Received: 25 June 2017 / Accepted: 4 October 2017 / Published online: 14 October 2017

Abstract The inhibition effects of orange peel extract (OPE) on the Q235 carbon steel corrosion in CO_2-saturated and CO_2/H_2S coexistent brine solutions were investigated by potentiodynamic polarization, electrochemical impedance spectroscopy (EIS), X-ray photoelectron spectroscopy (XPS) and scanning electron microscopy (SEM) analyses. The electrochemical measurements show that OPE can effectively retard the corrosion of Q235 steel induced by CO_2 and CO_2/H_2S. OPE exhibited higher corrosion inhibition efficiency in CO_2-saturated brine solutions than in CO_2/H_2S coexistent brine solutions. Inhibition efficiencies of 97.6 and 73.1% were achieved with 1000 mg L^{-1} OPE in CO_2 and CO_2/H_2S brine solutions, respectively. The double-layer capacitance values of the working electrodes decreased remarkedly after OPE was added in the brine solutions and continued to decrease gradually with the increase of the dosage of OPE. OPE is rich in oxygen- and nitrogen-containing groups as revealed by Fourier transform infrared (FT-IR) analysis and functions via the adsorption of these groups on the steel surface according to the XPS analysis. The adsorption behavior of these OPE moieties follows the Langmuir adsorption isotherm.

Keywords Adsorption · Orange peel extract · CO_2 corrosion · CO_2/H_2S corrosion · Corrosion inhibitor

✉ Jingmao Zhao
jingmaozhao@126.com

[1] College of Material Science and Engineering, Beijing University of Chemical Technology, No. 15, Beisanhuan East Road, Chao Yang District, Beijing 100029, China

[2] Beijing Key Laboratory of Electrochemical Process and Technology for Materials, Beijing 100029, China

Introduction

In oil and gas industry, failure of steel tanks, pipelines and other equipment is primarily related to CO_2 and H_2S corrosion. The presence of H_2S can change the corrosivity of produced fluids as compared to CO_2 corrosion, which makes the corrosion more complicated [1–3]. Carbon steel is widely used in the petroleum industry due to its excellent mechanical properties and low cost [4]. Therefore, the development of CO_2 and CO_2/H_2S corrosion inhibition techniques of carbon steel is of great importance.

Injecting organic corrosion inhibitors is usually a cost-effective and simple method to inhibit corrosion. The organic compounds containing heteroatoms including N, O, P and S possess potential corrosion inhibition properties [5–7]. However, the use of some organic inhibitors is gradually restricted due to their potential pollution to the environment.

To develop nontoxic and environmentally friendly corrosion inhibitors, the corrosion inhibition abilities of plant extracts have been extensively studied. The extracts of various plant parts, such as seeds [8–10], leaves [11, 12], flowers [13, 14] and fruits [15–17] have been found to possess excellent corrosion inhibition abilities which retard steel corrosion, mostly in inorganic acid solutions, such as HCl and H_2SO_4 [9, 12, 14–16], but rarely in CO_2 [17–19] or CO_2/H_2S solutions. Therefore, it is necessary to develop green CO_2 or CO_2/H_2S corrosion inhibitors from natural products.

Fruit peel is usually the by-product of processing food, such as fruit juices, and many scholars have researched the corrosion inhibition abilities of these fruit peel extracts. Sangeetha et al. [20] reported the corrosion inhibition behaviors of banana peel extracts in HCl solutions. Behpour et al. [21] discovered the inhibitive effects of punica granatum peel extract on the corrosion of steel in HCl and H_2SO_4 solutions. In addition, the corrosion inhibition abilities of the extracts of citrus aurantium peel [22], musa paradisiac peel [23] and musa sapientum peel [24] have also been studied. Therefore, fruit peel extracts have proven to be potential corrosion inhibitors in CO_2- and CO_2/H_2S-containing systems.

Orange peel is rich in pectin, hesperidin, polyphenols, carotenoids and vitamins etc. These compounds contain abundant heteroatoms, such as O and N atoms. Based on the structural characteristics of these compounds, it is anticipated that the orange peel extract (OPE) is a potential corrosion inhibitor. Saleh et al. [25] found the inhibitive effects of OPE on the corrosion of mild steel in HCl and H_2SO_4 solutions. Rocha et al. [16] and M'hiri et al. [26] discovered the corrosion inhibition behaviors of OPE on carbon steels in HCl solutions. Based on these reports, it can be concluded that OPE is a good corrosion inhibitor in acidic solutions. Both CO_2 and CO_2/H_2S corrosions are acid corrosion [27], therefore, OPE has a potential to retard the corrosion of carbon steels in brine solutions containing CO_2 or CO_2/H_2S.

The aim of the present work was to investigate the carbon steel corrosion inhibition performance of OPE in CO_2-saturated and CO_2/H_2S co-existent brine solutions by electrochemical measurements and to infer the inhibition mechanism by Fourier transform infrared spectroscopy (FT-IR) and X-ray photoelectron

spectroscopy (XPS) analyses. The surface morphologies of the samples were imaged via scanning electron microscopy (SEM).

Experimental methods

Materials

Q235 steels composed of (wt%) 0.19 C, 0.59 Mn, 0.3 Si, 0.044% P, 0.05 S and bal. Fe were cut into coupons with the sizes of 10 × 10 × 3 mm for electrochemistry measurements, 5 × 5 × 2 mm for XPS analysis and 50 × 10 × 3 mm for surface morphology imaging. The coupons were wet abraded with abrasive papers up to 2000 grit, degreased in acetone, rinsed with ethanol and dried by hot air.

Orange peel was dried in an oven at 50 °C for 12 h, smashed, and ground to a powder. 5 g of orange peel were extracted with 100 g of 50% ethanol solution at 60 °C for 2 h. The extraction solution was filtered, and dried by evaporation to achieve an OPE powder. The extract was kept in a desiccator before use.

The aggressive solution, 3.5 wt% NaCl solution, was prepared with analytical grade sodium chloride and distilled water.

Fourier transform infrared (FT-IR) spectroscopy

The FT-IR spectrum of OPE was recorded on a Nicolet-6700 spectrophotometer using KBr pellets in transmittance mode (Fig. 1). The peaks at 3414.9, 2930.3 and 1629.0 cm^{-1} are assigned to the –OH stretching, C–H stretching/OH group and ketonic stretching, respectively. The peak at 1517.7 cm^{-1} is attributed to the imino group. The ester stretching and C–O stretching result in the peaks at 1409.7 and

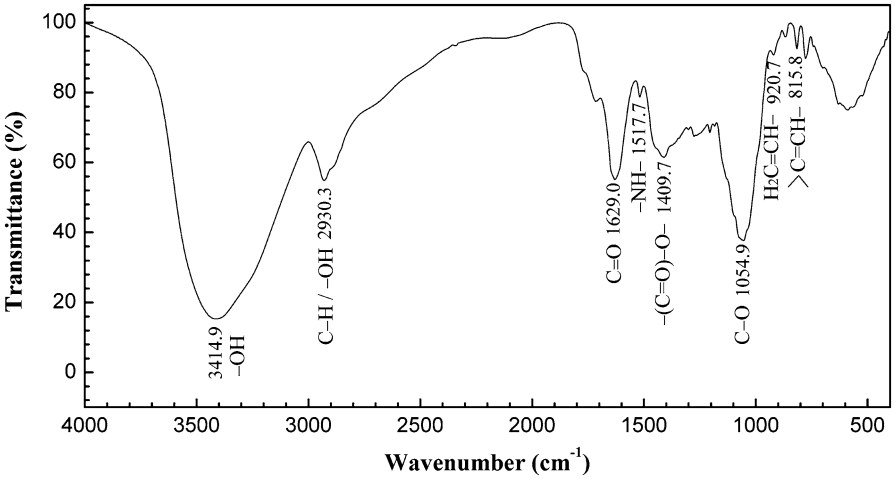

Fig. 1 FT-IR spectrum of OPE

1054.9 cm^{-1}, respectively. The single substituted and tri-substituted olefins can be determined by the peaks at 920.7 and 815.8 cm^{-1}, respectively.

Electrochemical measurements

The electrochemical measurements were carried out in a conventional three-electrode glass cell containing 200 mL of corrosive solution using a Gamry Interface 1000 electrochemical system at 60 ± 1 °C. A platinum foil and a saturated calomel electrode were used as the counter electrode and reference electrode, respectively. The CO_2-saturated brine solution was prepared by bubbling a 3.5 wt% NaCl solution with CO_2 for 1 h. Similarly, the CO_2/H_2S coexistent brine solution was obtained by bubbling a mixture of H_2S (20 mL min^{-1}) and CO_2 (20 mL min^{-1}) through the NaCl solution for 20 min. Electrochemical measurements were started after the Q235 steel (working electrode) was immersed in the test solution for 1 h to achieve a stable status. Figures 2a and 3a show the variations of open-circuit potential (OCP) versus immersion time measured on the Q235 steel

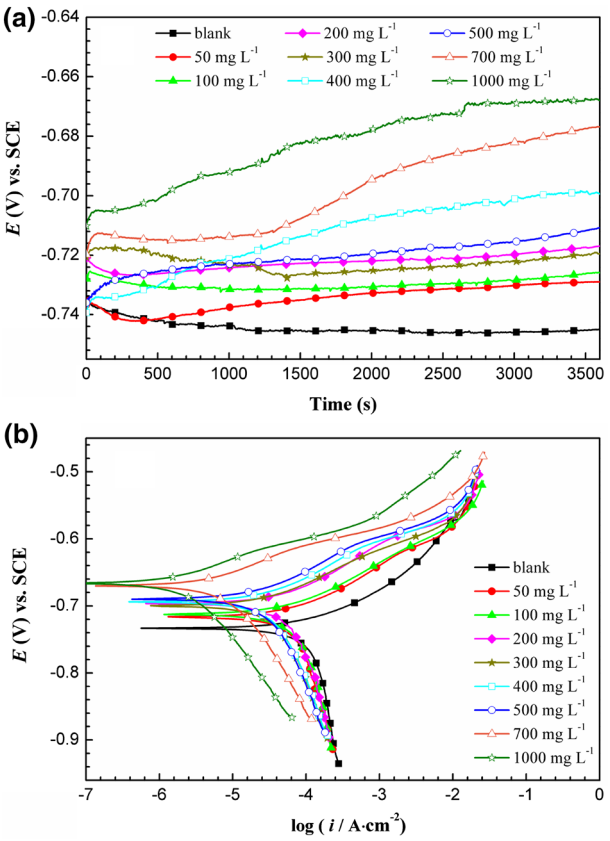

Fig. 2 OCP-time curves (**a**) and polarization curves (**b**) measured on Q235 steel electrode in the CO_2-saturated brine solutions containing various concentrations of OPE at 60 °C

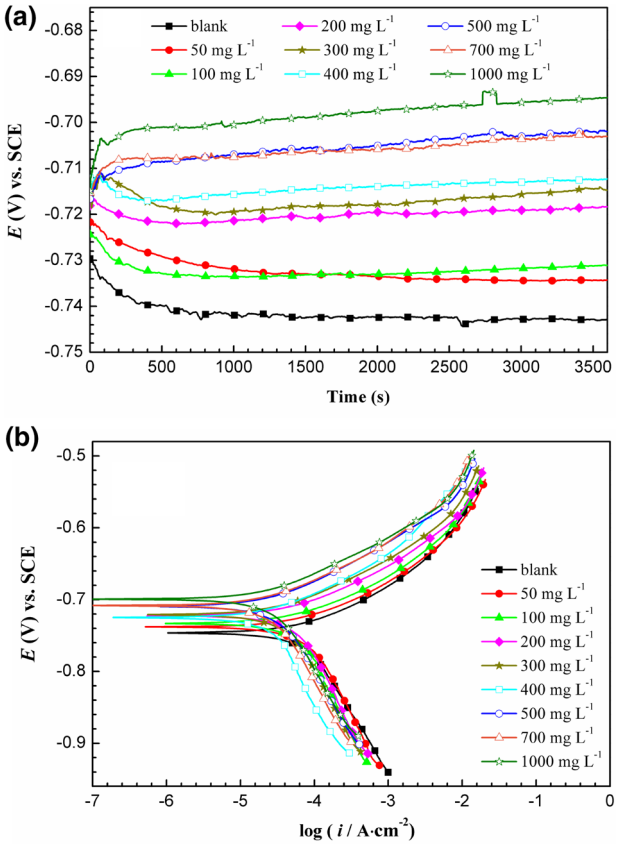

Fig. 3 OCP-time curves (**a**) and polarization curves (**b**) measured on Q235 steel electrode in the CO_2/H_2S coexistent brine solutions containing various concentrations of OPE at 60 °C

electrode in the CO_2-saturated and CO_2/H_2S co-existent brine solutions in the presence and absence of OPE, respectively. It was found that a steady-state OCP could be obtained in 1 h with the fluctuation less than ± 5 mV.

The potentiodynamic polarization measurements were conducted in the potential range from − 200 to + 200 mV versus OCP at the scan rate of 0.16 mV s^{-1}. The electrochemical parameters including corrosion potential (E_{corr}), anodic Tafel slope (β_a), cathodic Tafel slope (β_c) and corrosion current density (i_{corr}) were obtained by fitting the polarization curves in the Cview software. The inhibition efficiency (η_p) of OPE was calculated as follows

$$\eta_p = \frac{i_{corr} - i_{corr(OPE)}}{i_{corr}} \times 100\% \quad (1)$$

where i_{corr} and $i_{corr(OPE)}$ are the corrosion current densities in the absence and presence of OPE, respectively.

The electrochemical impedance spectroscopy (EIS) measurements were conducted in the frequency range from 100 kHz to 0.01 Hz with a perturbation amplitude of 5 mV versus OCP. The impedance data were fitted in the software Zsimpwin to estimate the inhibition efficiency (η_z) using Eq. (2)

$$\eta_Z = \frac{R_{t(OPE)} - R_t}{R_{t(OPE)}} \times 100\% \quad (2)$$

where R_t and $R_{t(OPE)}$ are the total resistances in the absence and presence of OPE, respectively.

Each measurement was repeated three or four times to ensure a good repeatability.

X-ray photoelectron spectroscopy (XPS) analysis

Steel coupons were immersed in CO_2-saturated or CO_2/H_2S coexistent brine solution containing 1000 mg L^{-1} OPE at 60 ± 1 °C for 24 h, taken out from the solution, dried by hot air and kept in a desiccator to prevent oxidation. XPS analysis was performed on a PHI-5300ESCA spectrometer (Perkin–Elmer, USA) equipped with an Al Kα excitation source. The binding energy of the C1s peak at 284.6 eV was used to calibrate all binding energies. The software XPSPEAK was used to fit and analyze XPS data.

Surface morphology observation

Steel coupons were immersed in CO_2-saturated or CO_2/H_2S coexistent brine solutions with or without OPE (1000 mg L^{-1}) at 60 ± 1 °C for 24 h, and treated as described in the "X-ray photoelectron spectroscopy (XPS) analysis" section. The surface morphologies of the coupons were then imaged via SEM (Quanta 200 F field, FEI Inc.).

Results and discussion

Potentiodynamic polarization measurements

The corrosion inhibition performances of OPE in CO_2-saturated and CO_2/H_2S coexistent brine solutions were evaluated by the potentiodynamic polarization measurements at 60 ± 1 °C. As shown in Figs. 2b and 3b, the polarization curves shifted towards lower current density values as different concentrations of OPE (c_{OPE}) were added, indicating that the inhibitive action of OPE, and the corrosion potential (E_{corr}) moved towards the positive direction. All of the displacements in E_{corr} are less than 85 mV, suggesting that OPE is a mixed-type inhibitor in both CO_2-saturated and CO_2/H_2S coexistent brine solutions [28, 29].

The curves measured in CO_2/H_2S coexistent brine solutions with 400–1000 mg L^{-1} OPE contains three different anodic slopes (Fig. 2a), suggesting

that different dissolution reactions took place over different potential ranges. The adsorption of OPE resulted in the first anodic slope. The second and the third anodic slopes sequentially appeared with the increase of potential due to the weak and significant desorptions of the absorbed OPE [30].

Three regions can be observed in the polarization curve according to the applied potential, including a linear region, followed by a weak polarization region and a strong polarization region (also known as the Tafel region). In the linear region, a lower potential is applied on the working electrode, typically ± 10 mV versus OCP, and the overpotential (ΔE) and current density (i) are linearly related. The fluctuation of OCP can significantly affect the measurements due to the low overpotential. In the strong polarization region with the overpotentials over 80 mV versus OCP, ΔE has a linear relationship with the logarithm of current density. The applied potential in the range between ± 10 and ± 70 mV versus OCP forms the weak polarization region where the measurement imparts less disturbance to the electrode system than in the strong polarization region. In addition, more reliable/accurate results can be achieved without the Tafel slope required. Various electrochemical parameters can thus be obtained by analyzing the experimental data of the linear, weak and strong polarization regions on the polarization curve. In the present work, the electrochemical parameters, including anodic Tafel slope (β_a), cathodic Tafel slope (β_c) and corrosion current density (i_{corr}), were achieved by fitting the experimental data in the weak polarization region in the software Cview by the nonlinear least square method. Tables 1 and 2 list the electrochemical parameters and inhibition efficiencies (η_p) calculated by Eq. (1). As shown in Table 1, η_p rapidly increases with the increase of the concentration of OPE (c_{OPE}) in the CO_2-saturated brine solution. In contrast, in the CO_2/H_2S coexistent brine solution, η_p increased initially with OPE concentration and became constant at c_{OPE} higher than 400 mg L^{-1}. Inhibition efficiencies of 97.6 and 73.1% were achieved with 1000 mg L^{-1} OPE in the CO_2 and CO_2/H_2S systems, respectively. These results indicate that OPE was able to effectively retard the corrosion of carbon steel

Table 1 Electrochemical parameters obtained by fitting the polarization curves of Q235 steel in the CO_2-saturated brine solutions containing various concentrations of OPE at 60 °C

c_{OPE} (mg L^{-1})	β_a (mV/dec)	β_c (mV/dec)	E_{corr} versus SCE (mV)	i_{corr} (μA/cm^2)	η_p (%)
Blank	51.6 ± 2.3	− 301.0 ± 9.1	− 733.4 ± 5.1	116.8 ± 4.2	–
50	57.3 ± 2.2	− 189.9 ± 5.3	− 717.1 ± 4.7	65.6 ± 3.1	43.8 ± 4.7
100	56.7 ± 2.8	− 196.8 ± 7.2	− 712.3 ± 5.9	59.5 ± 2.9	49.1 ± 4.3
200	60.6 ± 2.5	− 161.4 ± 6.3	− 697.4 ± 4.2	48.4 ± 2.8	58.6 ± 3.9
300	60.8 ± 2.1	− 159.9 ± 5.8	− 700.4 ± 3.9	37.3 ± 2.1	68.1 ± 3.0
400	60.9 ± 2.0	− 159.2 ± 6.7	− 694.8 ± 5.8	32.5 ± 2.4	72.2 ± 3.1
500	61.2 ± 2.5	− 157.0 ± 5.8	− 689.7 ± 6.3	25.4 ± 1.9	78.3 ± 2.4
700	61.7 ± 2.7	− 153.6 ± 4.9	− 669.7 ± 5.2	7.9 ± 0.6	93.2 ± 0.8
1000	59.2 ± 2.0	− 171.7 ± 6.2	− 667.0 ± 4.8	2.8 ± 0.2	97.6 ± 0.3

Table 2 Electrochemical parameters obtained by fitting the polarization curves of Q235 steel in the CO_2/H_2S coexistent brine solutions containing various concentrations of OPE at 60 °C

c_{OPE} (mg L^{-1})	β_a (mV/dec)	β_c (mV/dec)	E_{corr} versus SCE (mV)	i_{corr} (μA/cm^2)	η_p (%)
Blank	56.6 ± 2.1	− 198.4 ± 7.8	− 746.5 ± 4.3	84.2 ± 3.1	–
50	55.9 ± 1.9	− 207.9 ± 6.2	− 738.8 ± 5.5	79.9 ± 2.8	31.6 ± 6.8
100	52.2 ± 2.5	− 282.5 ± 8.4	− 733.4 ± 6.1	66.5 ± 2.5	43.1 ± 5.9
200	54.9 ± 2.2	− 222.9 ± 8.9	− 722.5 ± 7.4	59.2 ± 2.3	49.3 ± 5.3
300	56.3 ± 1.9	− 201.8 ± 7.1	− 721.8 ± 6.9	44.0 ± 1.9	62.3 ± 4.2
400	54.8 ± 1.8	− 223.6 ± 9.2	− 725.9 ± 8.3	31.5 ± 2.0	73.0 ± 3.8
500	58.1 ± 2.3	− 181.7 ± 6.3	− 709.1 ± 7.5	32.6 ± 1.6	72.1 ± 3.3
700	57.2 ± 2.4	− 190.8 ± 7.8	− 708.1 ± 5.9	30.1 ± 1.9	74.2 ± 3.6
1000	59.1 ± 1.7	− 172.4 ± 6.2	− 700.3 ± 8.3	31.4 ± 2.1	73.1 ± 3.9

in both CO_2-saturated and CO_2/H_2S coexistent brine solutions, but more effectively in the former.

Adsorption isotherm behaviour

The adsorption of an inhibitor on a steel surface can be considered as a substitutional process [31, 32]. The inhibition efficiency is proportional to the surface coverage (θ) that can be calculated with $\theta = \eta_p/100$. In both CO_2-saturated and CO_2/H_2S coexistent brine solutions, c_{OPE} exhibited a linear relationship with c_{OPE}/θ with a slope of almost unity as shown in Fig. 4. This behavior demonstrates that the moieties of OPE adsorbed onto the Q235 steel surface according to Langmuir adsorption isotherm, indicating a monomolecular adsorption of the adsorbed molecules and the absence of interactive forces between them. However,

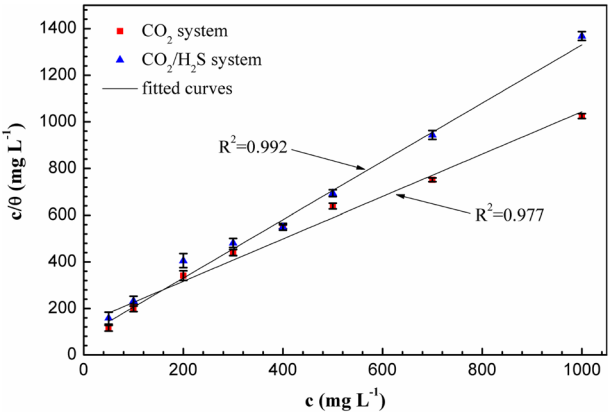

Fig. 4 Langmuir adsorption isotherms of OPE on Q235 steel in the CO_2-saturated and CO_2/H_2S coexistent brine solutions at 60 °C

some thermodynamic parameters, such as K and ΔG_{ads}, cannot be obtained due to the unknown molecular masses of the OPE components. Such limitations have been also noted elsewhere [16, 33].

EIS measurements

EIS measurements were performed to verify the inhibition effects of OPE on the Q235 steel corrosion in CO_2-saturated and CO_2/H_2S coexistent brine solutions at 60 ± 1 °C. As shown in Figs. 5a and 6a, all Nyquist plots contain a depressed semicircle at the high-frequency range, which is attributed to the roughness and other inhomogeneities of a solid surface [34, 35]. The diameters of the semicircles increased significantly after OPE was added in the CO_2-saturated and CO_2/H_2S coexistent brine solutions, indicating the good corrosion inhibition efficiency of OPE. Depressed semicircles were observed in some Nyquist plots at the low frequency range, which was attributed to the formation of corrosion product layer or inhibitor film. An inductive loop with an indication of a low-frequency blocking

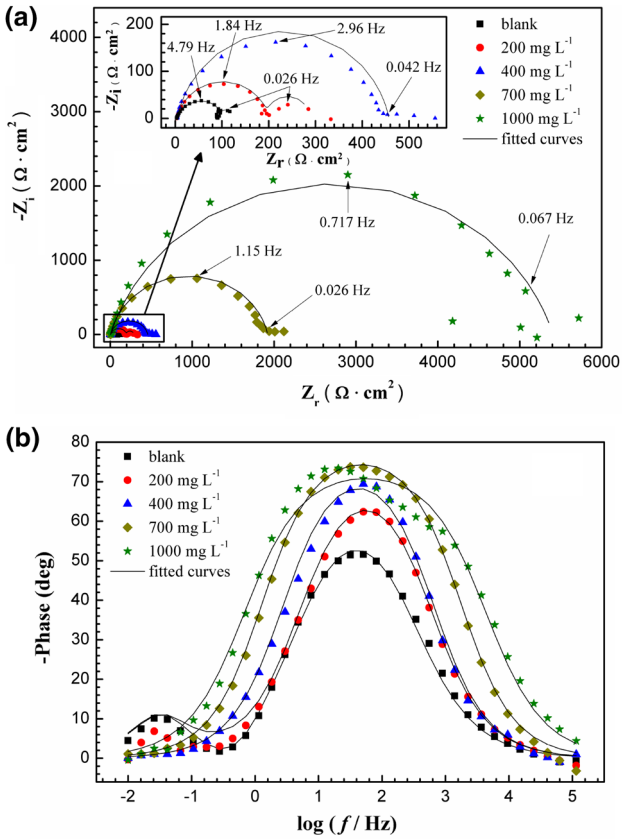

Fig. 5 **a** Nyquist and **b** Bode plots measured on Q235 steel in the CO_2-saturated brine solutions containing different concentrations of OPE at 60 °C

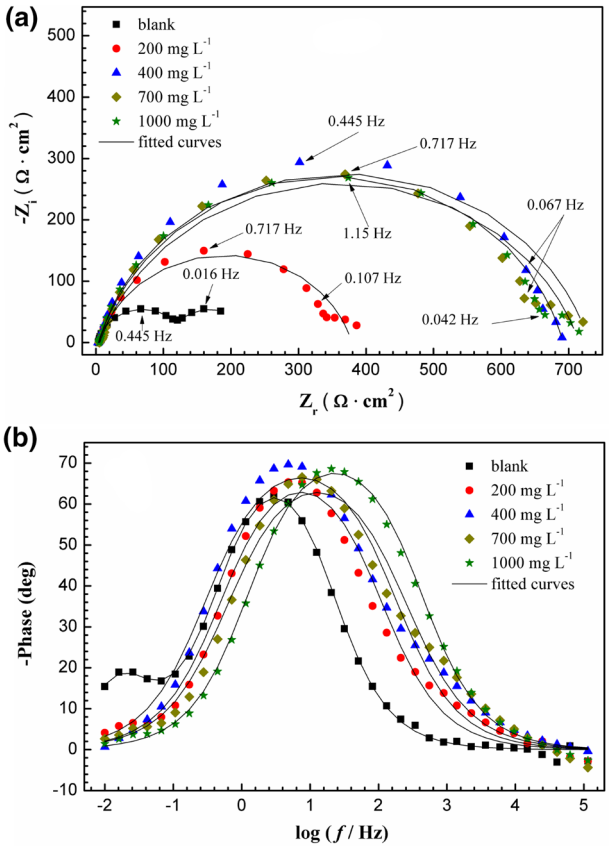

Fig. 6 **a** Nyquist and **b** Bode plots measured on Q235 steel in the CO_2/H_2S coexistent brine solutions containing different concentrations of OPE at 60 °C

feature was observed in the Nyquist plot measured without OPE in the CO_2 system. This blocking feature is due to the relaxation process of the adsorbent, such as H_{ads} or $FeOH_{ads}$ [36, 37].

Most Bode plots contain only one peak, and thus can be described by the one-time constant model (Fig. 7a) where R_s and R_{ct} are the solution and charge transfer resistances, respectively, and Q_{dl} is the constant phase element [38] (Figs. 5b and 6b). A few Bode plots can be described by the two-time constant models shown in Fig. 7b, c consisting of the resistance of the inhibitor film (R_f) or corrosion product layer (R_{cp}), the capacitance of inhibitor film (C_f) or corrosion product layer (C_{cp}), and the inductance (L) and its resistance (R_L).

The electrochemical parameters were obtained by fitting the impedance data (Tables 3 and 4), and the double layer capacitance (C_{dl}) was calculated as follows [39]:

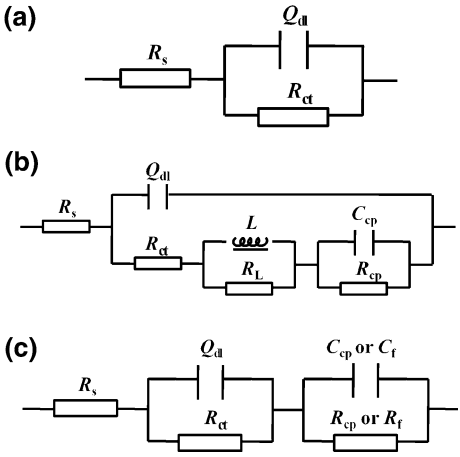

Fig. 7 Electrochemical equivalent circuits used to fit the impedance spectra measured on Q235 steel in the CO_2-saturated and CO_2/H_2S saturated brine solutions containing different concentrations of OPE at 60 °C

$$C_{dl} = Y^{1/n} R_{ct}^{(1-n)/n} \tag{3}$$

where Y and n are the magnitude of Q_{dl} and deviation parameter, respectively. C_{dl} can also be defined as follows [39, 40]:

$$C_{dl} = \frac{\varepsilon_0 \varepsilon}{d} S \tag{4}$$

where d is the thickness of the film, S is the surface area, ε_0 is the permittivity of the air and ε is the local dielectric constant. As shown in Tables 3 and 4, C_{dl} decreased remarkably after OPE was added to the CO_2-saturated and CO_2/H_2S coexistent brine solutions and continued to decrease gradually with the increase of the dosage of OPE because the adsorption of OPE on the steel surface decreased the local dielectric constant and/or increased the thickness of the inhibitor film [41].

The total resistance (R_t) in Tables 3 and 4 is equal to R_{ct} for the equivalent circuit in Fig. 7a, $R_{ct} + R_{cp} + R_L$ for the circuit in Fig. 7b, and $R_{ct} + R_{cp}$ or R_f for the circuit in Fig. 7c [42]. The inhibition efficiencies (η_Z) can be calculated by Eq. 2. It is clear that η_Z dramatically increased with the increase of c_{OPE} in the CO_2-saturated brine solution, and increased initially with the increase of c_{OPE} and became constant as c_{OPE} increased over 400 mg L^{-1} in the CO_2/H_2S coexistent brine solution. Therefore, it can be concluded that OPE can retard the corrosion of carbon steel in CO_2-saturated brine solutions more effectively than in CO_2/H_2S coexistent brine solutions, consistent with the conclusion drawn from potentiodynamic polarization measurements.

XPS analysis

As concluded above, OPE is an excellent corrosion inhibitor in both CO_2-saturated and CO_2/H_2S coexistent brine solutions. To explore its corrosion inhibition mechanism, XPS measurements were performed.

Table 3 Electrochemical parameters obtained by fitting the impedance data of Q235 steel in the CO_2-saturated brine solutions containing different concentrations of OPE at 60 °C

c_{OPE} (mg L^{-1})	Circuit	R_s (Ω cm^2)	Q_{dl}		C_{dl} (μF cm^{-2})	R_{ct} (Ω cm^2)	L (H cm^2)	R_L (Ω cm^2)	C_{cp} or C_f (F cm^{-2})	R_{cp} or R_f (Ω cm^2)	R_t (Ω cm^2)	η_z (%)
			Y ($\mu\Omega^{-1}$ cm^{-2} S^n)	n								
Blank	(b)	3.28 ± 0.23	728.0 ± 43.2	0.80 ± 0.03	355.6 ± 77.7	74.5 ± 3.2	4.93 ± 0.29	16.3 ± 0.7	0.160 ± 0.007	36.6 ± 2.1	127.4 ± 6.0	–
200	(c)	3.43 ± 0.19	262.4 ± 10.5	0.85 ± 0.02	156.2 ± 21.2	196.7 ± 8.3	–	–	0.067 ± 0.002	87.6 ± 3.9	284.3 ± 12.2	55.2 ± 4.0
400	(a)	3.94 ± 0.21	182.3 ± 6.0	0.87 ± 0.03	125.9 ± 18.3	453.4 ± 29.2	–	–	–	–	453.4 ± 29.2	71.9 ± 3.1
700	(a)	3.48 ± 0.15	82.2 ± 4.7	0.88 ± 0.01	64.0 ± 6.1	1918 ± 89	–	–	–	–	1918 ± 89	93.4 ± 0.6
1000	(a)	4.10 ± 0.18	56.3 ± 3.4	0.82 ± 0.02	43.4 ± 5.1	5402 ± 216	–	–	–	–	5402 ± 216	97.6 ± 0.2

– Means the value for its corresponding element is nonexistent

Table 4 Electrochemical parameters obtained by fitting the impedance data of Q235 steel in the CO_2/H_2S coexistent brine solutions containing different concentrations of OPE at 60 °C

c_{OPE} (mg L^{-1})	Circuit	R_s (Ω cm^2)	Q_{dl}		C_{dl} (μF cm^{-2})	R_{ct} (Ω cm^2)	C_{cp} (F cm^{-2})	R_{cp} (Ω cm^2)	R_t (Ω cm^2)	η_z (%)
			Y ($\mu\Omega^{-1}$ cm^{-2} S^n)	n						
Blank	(c)	4.05 ± 0.25	3160 ± 189	0.90 ± 0.02	2853.8 ± 270.2	127.5 ± 6.7	0.131 ± 0.004	93.2 ± 4.3	220.7 ± 11.0	–
200	(a)	2.65 ± 0.17	1025 ± 69	0.83 ± 0.02	842.6 ± 98.4	374.4 ± 14.8	–	–	374.4 ± 14.8	41.0 ± 5.3
400	(a)	2.26 ± 0.13	805.4 ± 32.2	0.82 ± 0.03	714.3 ± 59.3	727.0 ± 34.2	–	–	727.0 ± 34.2	69.6 ± 2.9
700	(a)	3.44 ± 0.22	461.2 ± 18.4	0.80 ± 0.02	348.8 ± 33	709.8 ± 28.4	–	–	709.8 ± 28.4	68.9 ± 2.8
1000	(a)	2.43 ± 0.18	254.7 ± 12.5	0.85 ± 0.01	187.4 ± 16.2	686.8 ± 18.1	–	–	686.8 ± 18.1	67.9 ± 2.5

– Means the value for its corresponding element is nonexistent

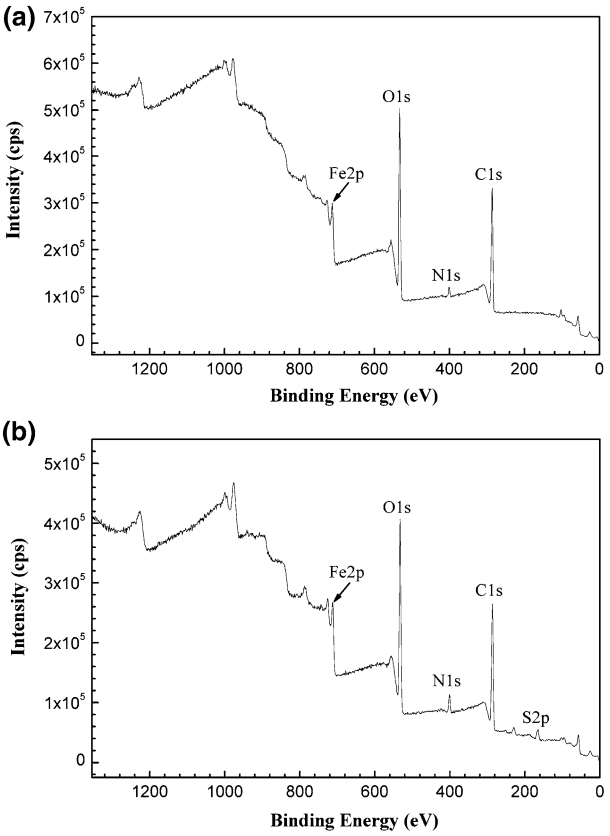

Fig. 8 Wide-scan XPS spectra of Q235 steel immersed in the CO_2-saturated (**a**) and CO_2/H_2S coexistent (**b**) brine solutions containing 1000 mg L^{-1} OPE for 24 h at 60 °C

Figure 8 shows the wide-scan XPS spectra of Q235 steels immersed in the CO_2-saturated and CO_2/H_2S coexistent brine solutions containing 1000 mg L^{-1} OPE for 24 h at 60 °C, respectively. The peaks of C1s, N1s, O1s and Fe2p were observed on both spectra, and the S2p peak only appeared on the spectrum of the steel samples immersed in CO_2/H_2S coexistent brine solution (Fig. 8b). The signals of C1s, N1s and O1s were mainly attributed to the adsorbed components of OPE on the steel surface, and the Fe2p peak was due to the iron matrix and its corrosion products. The signal of S2p suggests the formation of iron sulfide.

The high-resolution C1s spectra contains four peaks associated with the C–C and C–H peak at 284.6 eV [43], C–N and C–O peak at 286.0 eV [43, 44], C=O peak at 287.8 eV [43, 45] and COOR and $FeCO_3$ peak at 288.9 eV [46, 47] (Fig. 9). Only one peak at 400.0 eV was observed on the high-resolution spectra of N1s, which could be assigned to C–NH–R [44] (Fig. 10). Figure 11 shows the high-resolution spectra of O1s consisting of three peaks. The peak at 531.2 eV was attributed to the

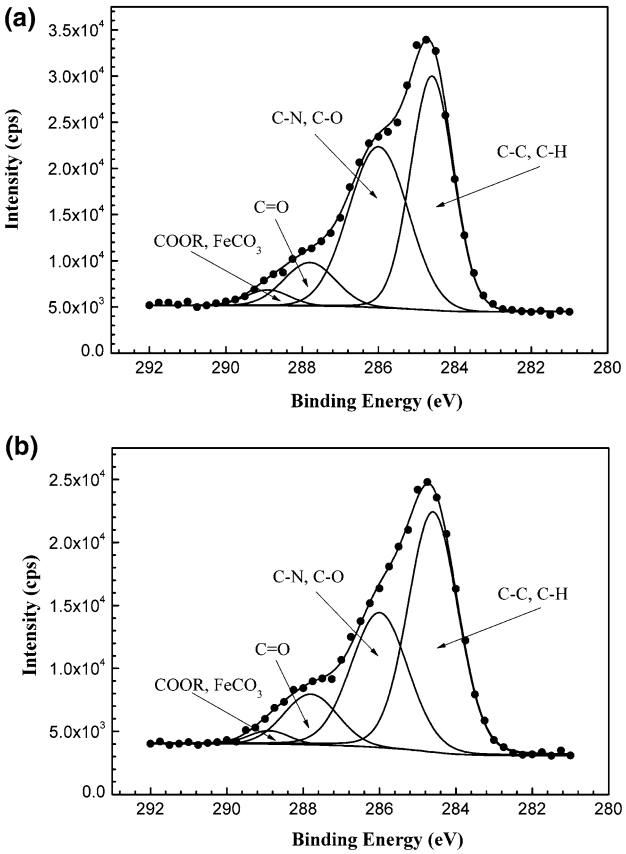

Fig. 9 High-resolution C1s spectra of Q235 steel immersed in the CO_2-saturated (**a**) and CO_2/H_2S coexistent (**b**) brine solutions containing 1000 mg L^{-1} OPE for 24 h at 60 °C

C=O group [47, 48] and the peak at 532.7–533.0 eV could be assigned to the C–O bonds in ethers, hydroxyls and esters [48, 49]. The peak at 533.8–534.0 eV indicates the presence of ether oxygen atoms in esters and anhydrides [48, 50, 51].

Surface morphology analysis

The surface morphologies of the steel coupons immersed in CO_2-saturated and CO_2/H_2S coexistent brine solutions in the absence and presence of OPE (1000 mg L^{-1}) were imaged using SEM. The steel surfaces were severely corroded in the CO_2-saturated and CO_2/H_2S coexistent solutions with no OPE (Fig. 12a, b). After 1000 mg L^{-1} OPE added to the solutions, the corrosion caused by the corrosive media was remarkably reduced (Fig. 12c, d), indicating the excellent corrosion inhibition ability of OPE in both CO_2-saturated and CO_2/H_2S coexistent brine solutions. In addition, in the presence of 1000 mg L^{-1} OPE, the steel surface

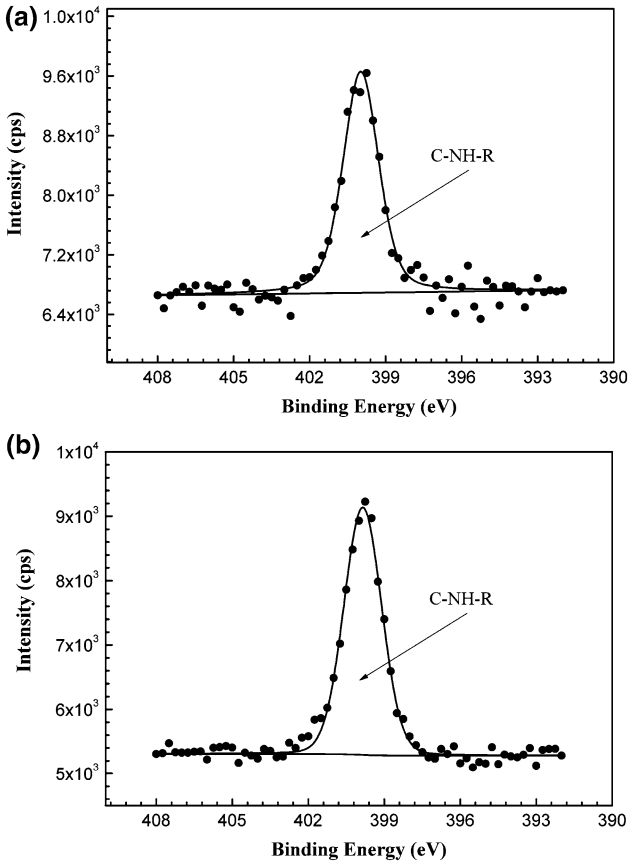

Fig. 10 High-resolution N1s spectra of Q235 steel immersed in the CO_2-saturated (**a**) and CO_2/H_2S coexistent (**b**) brine solutions containing 1000 mg L^{-1} OPE for 24 h at 60 °C

immersed in the CO_2-saturated brine solution is smoother than that immersed in the CO_2/H_2S coexistent brine solution.

Discussion

The potentiodynamic polarization and EIS measurements suggest that the corrosion of Q235 steel induced by CO_2 and CO_2/H_2S was effectively retarded by OPE via adsorption on the steel surface. The adsorption followed the Langmuir adsorption isotherm. Orange peel is rich in pectin, organic acids and antioxidant compounds, such as polyphenols, carotenoids and vitamins [16, 25]. Although the corrosion inhibition properties of some organic compounds, such as phenolics [52] and tannic acid (an organic acid) [53] have been reported, it is still a challenge to assign the corrosion inhibition property of OPE to one or more particular constituents because

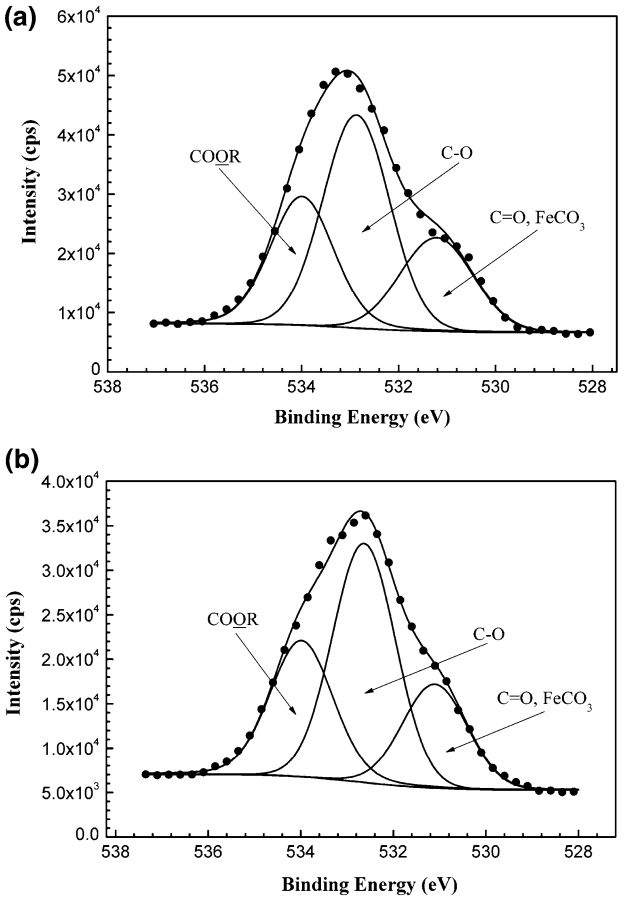

Fig. 11 High-resolution O1s spectra of Q235 steel immersed in the CO_2-saturated (**a**) and CO_2/H_2S coexistent (**b**) brine solutions containing 1000 mg L^{-1} OPE for 24 h at 60 °C

of the complex compositions of OPE. FT-IR analysis suggests abundant oxygen-containing groups and less nitrogen-containing groups in OPE. XPS analysis revealed hydroxyl, ether, carbonyl, ester and imino groups adsorbed on the steel surface. O and N atoms can donate their lone electron pairs to form coordinate covalent bonds with Fe atoms [54]. Therefore, it can be concluded that the corrosion inhibition property of OPE is due to the strong adsorption of the N- and O-containing organic moieties of OPE on the steel surface.

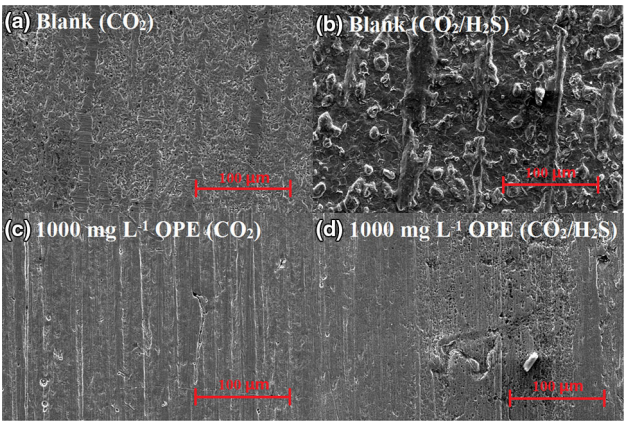

Fig. 12 SEM images of the surfaces of Q235 steel samples immersed in the CO_2-saturated brine solution in the absence (**a**) and presence (**c**) of OPE (1000 mg L^{-1}), and the surfaces of coupons immersed in the CO_2/H_2S coexistent brine solution in the absence (**b**) and presence (**d**) of OPE (1000 mg L^{-1})

Conclusions

In the present work, OPE was demonstrated as a mixed-type inhibitor which significantly retards the corrosions of Q235 steel in CO_2-saturated and CO_2/H_2S coexistent brine solutions. OPE exhibited a better corrosion inhibition efficiency in CO_2-saturated brine solutions than in CO_2/H_2S coexistent brine solutions. Inhibition efficiencies of 97.6 and 74.2% were achieved with 1000 mg L^{-1} OPE in CO_2 and CO_2/H_2S systems, respectively. OPE effectively decreased the double-layer capacitances in the two systems by forming inhibitor films on the steel surface. OPE is rich in oxygen- and nitrogen-containing groups, and the inhibition effect of OPE on the corrosion of Q235 steel is due to the adsorption of these groups on the steel surface. The adsorption follows the Langmuir adsorption isotherm.

Acknowledgements The authors would like to thank the National Natural Science Foundation of China for the financial supports for this work (No. 51471021).

References

1. P. Rajeev, A.O. Surendranathan, C.S.N. Murthy, J. Mater. Environ. Sci. **3**, 856 (2012)
2. S.N. Smith, M.W. Joosten, *Corrosion of Carbon Steel by H_2S in CO_2 Containing Oilfield Environments, Corrosion 2006* (NACE International, San Diego, 2006)
3. S.N. Smith, M.W. Joosten, *Corrosion of Carbon Steel by H_2S in CO_2 Containing Oilfield Environments-10 Year Update, Corrosion 2015* (NACE International, Dallas, 2015)
4. F.E.T. Heakal, A.E. Elkholy, J. Mol. Liq. **230**, 395 (2017)
5. M. Elachouri, M.S. Hajji, S. Kertit, E.M. Essassi, M. Salem, R. Coudert, Corros. Sci. **37**, 381 (1995)
6. G. Schmitt, Br. Corros. J. **19**, 165 (1984)
7. B. Mernari, H. El Attari, M. Traisnel, F. Bentiss, M. Lagrenee, Corros. Sci. **40**, 391 (1998)
8. R.M. Saleh, A.A. Ismail, A.A. El Hosary, Corros. Sci. **23**, 1239 (1983)
9. F. Zucchi, I.H. Omar, Surf. Technol. **24**, 391 (1985)
10. P.C. Okafor, M.E. Ikpi, I.E. Uwah, E.E. Ebenso, U.J. Ekpe, S.A. Umoren, Corros. Sci. **50**, 2310 (2008)

11. T. Ibrahim, H. Alayan, Y. Al, Mowaqet. Prog. Org. Coat. **75**, 456 (2012)
12. M. Kliškić, J. Radošević, S. Gudić, V. Katalinić, J. Appl. Electrochem. **30**, 823 (2000)
13. C.B.P. Kumar, K.N. Mohana, Egypt. J. Pet. **23**, 201 (2014)
14. A. Ostovari, S.M. Hoseinieh, M. Peikari, S.R. Shadizadeh, S.J. Hashemi, Corros. Sci. **51**, 1935 (2009)
15. C.M. Reddy, B.D. Sanketi, S.N. Kumar, Perspect. Sci. **8**, 603 (2016)
16. J.C. da Rocha, J.A.C.P. Gomes, E. D'Elia, Corros. Sci. **52**, 2341 (2010)
17. A. Singh, Y. Lin, W. Liu, D. Kuanhai, J. Pan, B. Huang, C. Ren, D. Zeng, J. Taiwan Inst. Chem. Eng. **45**, 1918 (2014)
18. J. Zhao, H. Duan, R. Jiang, Int. J. Electrochem. Sci. **10**, 2716 (2015)
19. A. Singh, Y. Lin, E.E. Ebenso, W. Liu, J. Pan, B. Huang, J. Ind. Eng. Chem. **24**, 219 (2015)
20. M. Sangeetha, S. Rajendran, J. Sathiyabama, P. Prabhakar, J. Nat. Prod. Plant Resour. **2**, 601 (2012)
21. M. Behpour, S.M. Ghoreishi, M. Khayatkashani, N. Soltani, Mater. Chem. Phys. **131**, 621 (2012)
22. H. Elmsellem, H. Bendaha, A. Aouniti, A. Chetouani, M. Mimouni, A. Bouyanzer, Mor. J. Chem. **2**, 1 (2014)
23. G. Ji, S. Anjum, S. Sundaram, R. Prakash, Corros. Sci. **90**, 107 (2015)
24. S. Africa, Afr. J. Pure Appl. Chem. **2**, 46 (2008)
25. R.M. Saleh, A.A. Ismall, A.A. El Hosary, Br. Corros. J. **17**, 131 (1982)
26. N. M'hiri, D. Veys-Renaux, E. Rocca, I. Ioannou, N.M. Boudhrioua, M. Ghoul, Corros. Sci. **102**, 55 (2016)
27. J.L. Crolet, J. Pet. Technol. **35**, 1553 (1983)
28. A. Singh, Y. Lin, I.B. Obot, E.E. Ebenso, J. Mol. Liq. **219**, 865 (2016)
29. E.S. Ferreira, C. Giacomelli, F.C. Giacomelli, A. Spinelli, Mater. Chem. Phys. **83**, 129 (2004)
30. P.C. Okafor, Y. Zheng, Corros. Sci. **51**, 850 (2009)
31. B.G. Ateya, B.E. El-Anadouli, F.M. El-Nizamy, Corros. Sci. **24**, 509 (1984)
32. A.A. El-Awady, B.A. Abd-El-Nabey, S.G. Aziz, J. Electrochem. Soc. **139**, 2149 (1992)
33. L. Valek, S. Martinez, Mater. Lett. **61**, 148 (2007)
34. K. Jüttner, Electrochim. Acta **35**, 1501 (1990)
35. T. Pajkossy, J. Electroanal. Chem. **364**, 111 (1994)
36. M. Lebrini, M. Lagrenee, H. Vezin, L. Gengembre, F. Bentiss, Corros. Sci. **47**, 485 (2005)
37. G. Zhang, C. Chen, M. Lu, C. Chai, Y. Wu, Mater. Chem. Phys. **105**, 331 (2007)
38. A.V. Benedeti, P.T.A. Sumodjo, K. Nobe, P.L. Cabot, W.G. Proud, Electrochim. Acta **40**, 2657 (1995)
39. B. Hirschorn, M.E. Orazem, B. Tribollet, V. Vivier, I. Frateur, M. Musiani, Electrochim. Acta **55**, 6218 (2010)
40. L. Hamadou, A. Kadri, N. Benbrahim, Appl. Surf. Sci. **252**, 1510 (2005)
41. A.K. Singh, M.A. Quraishi, Corros. Sci. **52**, 152 (2010)
42. M.V. Azghandi, A. Davoodi, G.A. Farzi, A. Kosari, Corros. Sci. **64**, 44 (2012)
43. S. Delpeux, F. Beguin, R. Benoit, R. Erre, N. Manolova, I. Rashkov, Eur. Polym. J. **34**, 905 (1998)
44. O. Olivares-Xometl, N.V. Likhanova, M.A. Dominguez-Aguilar, J.M. Hallen, L.S. Zamudio, E. Arce, Appl. Surf. Sci. **252**, 2139 (2006)
45. D. Briggs, G. Beamson, Anal. Chem. **64**, 1729 (1992)
46. T.R. Wang, J.L. Wang, Y.Q. Wu, Corros. Sci. **97**, 89 (2015)
47. J.K. Heuer, J.F. Stubbins, Corros. Sci. **41**, 1231 (1999)
48. R. Larciprete, S. Gardonio, L. Petaccia, S. Lizzit, Carbon **47**, 2579 (2009)
49. U. Zielke, K.J. Hüttinger, W.P. Hoffman, Carbon **34**, 983 (1996)
50. A. Rjeb, S. Letarte, L. Tajounte, M. Chafik El Idrissi, A. Adnot, D. Roy, Y. Claire, J. Kaloustian, J. Electron Spectrosc. **107**, 221 (2000)
51. S.N. Jampala, S. Manolache, S. Gunasekaran, F.S. Denes, J. Agric. Food Chem. **53**, 3618 (2005)
52. M. Abdallah, B.H. Asghar, I. Zaafarany, A.S. Fouda, Int. J. Electrochem. Sci. **7**, 282 (2012)
53. A.M. Beccaria, E.D. Mor, Br. Corros. J. **11**, 156 (1976)
54. N. Hackerman, A.C. Makrides, Ind. Eng. Chem. **46**, 523 (1954)